Experimental Characterization of Conducted EMI in Series Choppers: Common- and Differential-Mode Analysis in Accordance with EN55022

ABDESLAM LAHMANI[1], HOUCINE MILOUDI[1], MOHAMED MILOUDI[1,2], ABDELKADER GOURBI[1,3], MOHAMMED HAMZA BERMAKI[1], KHEIRA MENDAZ[4]

[1]APELEC Laboratory, Electrical Engineering Department,
Djillali Liabes University,
Sidi Bel Abbes,
ALGERIA

[2]GIDD Laboratory, Electrical Engineering, and Automation Department,
Ahmed Zabana - Relizane University,
Relizane,
ALGERIA

[3]Institute of Science and Applied Techniques,
Ahmed Ben Bella Oran 1 University,
Oran,
ALGERIA

[4]Electrical Engineering Department,
Belhadj Bouchaib University,
Ain Temouchent,
ALGERIA

Abstract: - Static converters have seen major advancements in efficiency and compactness, but remain a primary source of conducted and radiated electromagnetic disturbances, particularly during semiconductor switching events. These disturbances propagate through parasitic elements and must comply with electromagnetic compatibility (EMC) standards to ensure safe coexistence with other systems. This work presents a detailed experimental investigation of conducted electromagnetic interference (EMI) in a series chopper, with a focus on distinguishing and quantifying common-mode (CM) and differential-mode (DM) noise. Unlike studies that rely mainly on simulation or analytical modeling, this research emphasizes precise measurement techniques to capture both CM and DM emissions over the 150 kHz–30 MHz range, following EN55022 requirements. The effects of duty cycle and MOSFET switching characteristics on EMI levels are systematically examined. Results show that DM emissions dominate over CM across the measured spectrum, with certain configurations exceeding EN55022 Class A limits at low frequencies. The findings highlight the critical role of component selection and operating parameters in achieving EMC compliance, and provide practical insights for optimizing chopper design to mitigate conducted emissions.

Key-Words: - Static Converters, Chopper Series, Conducted EMI, Measurements, Common Mode, Differential Mode, EN55022 Compliance, Experimental Measurements.

Received: June 17, 2025. Revised: October 8, 2025. Accepted: January 11, 2026. Published: June 2, 2026.

1 Introduction

In recent years, significant research has been devoted to understanding and improving the electromagnetic compatibility (EMC) performance of electrical machines [1], [2], [3], [4], power electronics [5], [6], [7], and energy conversion systems [8], [9], [10]. Among these, electric motors have been extensively studied, both for their role as critical loads and for their contribution to electromagnetic interference (EMI) issues [11], [12], [13]. Various works have examined EMI generation in motors, focusing on the characterization of common-mode (CM) [14], [15] and differential-mode (DM) [16], [17], [18] disturbances, high-frequency modeling [19], [20], [21], and mitigation strategies to ensure compliance with EMC standards [22], [23], [24], [25]. These investigations highlight that motor systems—especially when fed by variable-speed drives—can be significant sources of conducted and radiated disturbances, which may negatively affect surrounding equipment [26], [27].

The growing integration of renewable energy sources [28] has further increased the demand for high-efficiency [29], low-noise power conversion systems, [30], [31]. Hybrid photovoltaic systems and wind energy applications, in particular, require compact and efficient power electronics to interface with the grid while maintaining strict EMC compliance, [32], [33]. The challenge lies in ensuring that the power converters used in renewable energy installations operate reliably under varying load and environmental conditions without exceeding EMI limits, [34], [35]. Studies have shown that both conducted and radiated EMI in renewable energy converters must be carefully managed to prevent interference with sensitive communication and control systems, [36], [37].

Static converters—such as choppers [38], buck-boost converters [39], and inverters—are now ubiquitous in motor control, renewable energy integration, and a wide range of industrial and consumer electronics applications, [40]. They provide improved energy efficiency, compact design, and precise control, but their high-speed switching of semiconductor devices inevitably leads to significant EMI generation, [41], [42], [43]. This has motivated a large body of research into modeling, prediction, and experimental measurement of conducted and radiated disturbances in such systems, [44], [45], [46]. In particular, the separation and analysis of CM and DM noise are essential steps in understanding the propagation mechanisms of EMI and in designing appropriate mitigation strategies, [47], [48].

The buck converter is a step-down DC–DC power conversion circuit designed to reduce a higher input voltage to a lower output voltage. It is among the most widely used converter topologies in modern power electronic systems [49], including switched-mode power supplies (SMPS) [50], [51], smartphones [52], laptops [53], and battery chargers [54]. These converters typically employ high-speed semiconductor switching devices, such as MOSFETs and IGBTs, which enable rapid voltage (dv/dt) and/or current (di/dt) transitions, [55]. While such fast switching enhances efficiency and minimizes the converter's size, it also introduces substantial EMI, [56].

Depending on the propagation mechanism, EMI can be categorized into conducted disturbances—transmitted through electrical conduction—and radiated disturbances—propagated via electromagnetic fields in the surrounding medium [12], [15]. Conducted disturbances propagate in two distinct modes: DM and CM, [14], [15], [16], [17]. In DM, the converter produces a pulse-width modulated (PWM) voltage between system phases, with the current flowing through one phase and returning through another, [57]. In CM, the converter generates a voltage between each phase and ground, causing parasitic currents to flow in the same direction along the phases and return to the interference source via the system's parasitic capacitances and common-mode impedances.

The prediction and modeling of conducted EMI are typically performed using two main approaches. The time-domain approach employs circuit simulation tools such as Saber or SPICE to model the converter's operation in the time domain, after which the noise spectrum is obtained through a Fast Fourier Transform (FFT), [58]. The frequency-domain approach models and estimates the spectral content of the interference directly in the frequency domain, using either analytical models or experimental measurements, [11].

Before detailing the proposed methodology and findings, it is important to review relevant works on EMI modeling, prediction, and mitigation for DC–DC converters. Table 1 (Appendix) summarizes the main contributions from the literature, including converter types, EMI prediction methods, and mitigation strategies. This table serves as a foundation for positioning the present study within the broader context of EMI research in static power converters.

This paper focuses on the experimental characterization of CM and DM conducted EMI generated by a series chopper. While many previous studies have approached this topic through simulation or analytical modeling, the present work emphasizes direct measurement using an experimental setup in accordance with the EN55022 standard. The effects of key parameters—such as duty cycle and MOSFET switching characteristics—on EMI levels are systematically investigated. This analysis not only provides insight into the behavior of CM and DM noise but also evaluates the converter's compliance with EMC limits, thereby guiding design optimization for improved electromagnetic compatibility.

This paper addresses a gap in the literature by experimentally characterizing conducted EMI in a series chopper, with clear separation of CM and DM disturbances. Unlike prior studies relying on simulations or indirect models, this work uses precise EN55022-compliant measurements over 150 kHz–30 MHz to assess the effects of duty cycle and MOSFET switching characteristics on emission magnitude and spectrum. The systematic CM–DM comparison identifies dominant propagation mechanisms and evaluates EMC compliance, providing practical guidance for improving static converter performance in electromagnetically sensitive environments.

2 Measurement Setup of EMI

2.1 Realization of the Series Chopper Circuit

This section outlines the complete procedure followed in this study, from the construction of the series chopper to the configuration of the EMC test bench used for acquiring the required experimental measurements.

A chopper is a DC–DC power converter that transforms a fixed direct voltage or current into a variable direct voltage or current. The series chopper, in particular, is designed to regulate the output by controlling the duty cycle of the switching device. Its general configuration is illustrated in Figure 1, where the input DC source is connected in series with the switching element, filter components, and load. This arrangement enables step-up or step-down control of the output while maintaining high efficiency, making it suitable for precise EMI characterization under controlled operating conditions.

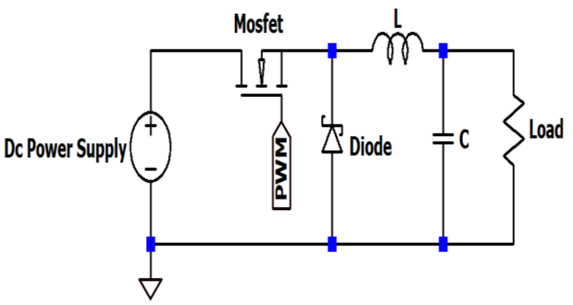

Fig. 1: General configuration of buck converter
Source: [59], [60]

The implemented series chopper circuit consists of a power diode (BYT12P600), a MOSFET switch (IRF840), a 1 kΩ resistive load, and two push-buttons for adjusting the chopper duty cycle. The circuit is powered by a 20 V DC input supply and delivers a variable output voltage, where the average value is directly dependent on the duty cycle of operation.

The converter is driven by a 5 V pulse-width modulation (PWM) signal generated by a PIC16F877A microcontroller. Since the MOSFET requires proper gate drive levels for reliable switching, a dedicated driver stage is employed to interface the PWM control signal with the power switch, [13].

The main components and layout of the realized series chopper are illustrated in Figure 2.

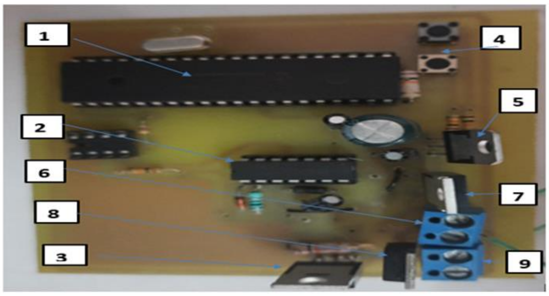

1. PIC16F78A 2. Driver IR2110 3.Mosfet IRF840
4. Push Buttons 5. Regulator 5V 6. Load terminal
7. Regulateur12V 8. BYT12P600 9. Power supply input

Fig. 2: Chopper circuit PCB
Source: [61]

The experimentally measured output voltage waveform of the implemented series chopper is shown in Figure 3. The waveform clearly demonstrates the expected PWM-controlled shape, where the average output voltage varies proportionally with the applied duty cycle. This confirms the proper operation of the chopper and validates the control strategy implemented through the PIC16F877A-based PWM generation.

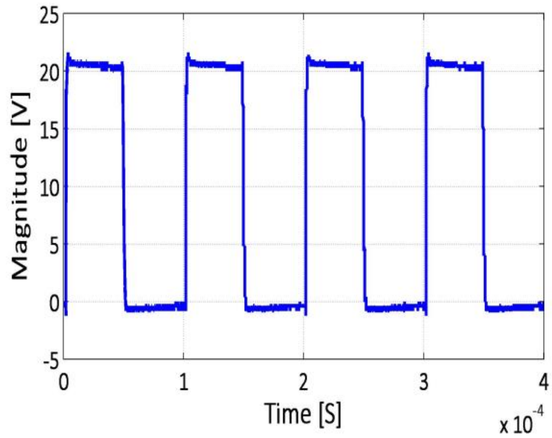

Fig. 3: Time-Domain Response of Series Chopper Output Voltage
Source: created by the authors

2.2 CM and DM Current Measurement Configuration

CM current flows through both conductors in the same direction with respect to a common reference, typically the ground, whereas DM current flows in opposite directions between two conductors, [30].

To accurately characterize the electromagnetic interference generated by the series chopper, specific measurement configurations must be adopted for each mode. Using a current probe, the CM and DM currents are measured by applying distinct setups tailored to their respective propagation characteristics. These configurations are illustrated in Figure 4.

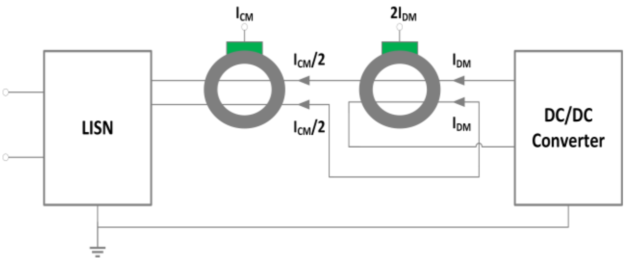

Fig. 4: Series chopper current measurement of common mode and differential mode
Source: [62], [63]

Once the disturbance currents (I_{DM} and I_{CM}) are measured, it is simply carried out to derive the corresponding disturbance voltages for each mode from the following conversion equations:

$V_{DM} = 100 \times I_{DM}$

$V_{CM} = 25 \times I_{CM}$

2.3 Experimental Measuring Bench

The experimental bench, illustrated in Figure 5, was designed to measure the conducted emissions of the implemented series chopper in compliance with the EN550022 standard. Measurements were performed over the frequency range of 150 kHz to 30 MHz.

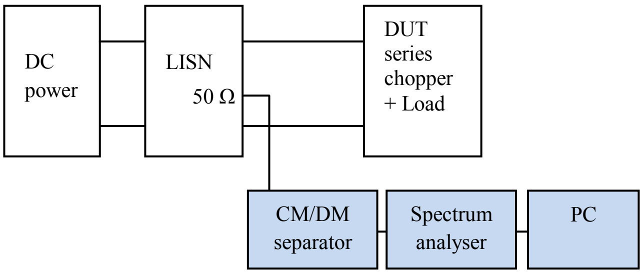

Fig. 5: Diagram of the test set-up used for measuring conducted emissions
Source: [64]

A Line Impedance Stabilization Network (LISN) was inserted between the DC power supply and the device under test (DUT) to isolate the power supply network from the converter under investigation. This configuration ensures measurement accuracy, compliance with EMC testing requirements, and operator safety.

The conducted EMI signals in the frequency domain were captured using a spectrum analyzer, while a current probe was employed to measure both CM and DM noise currents.

The schematic of the experimental bench setup and its corresponding photograph are presented in Figure 5 and Figure 6, respectively.

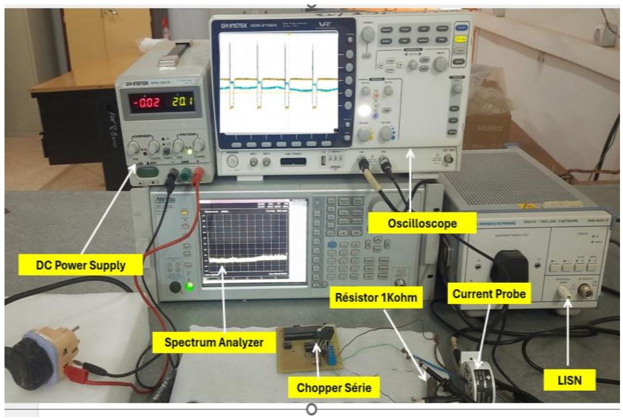

Fig. 6: Photograph of the measuring bench of the electromagnetic disturbances generated by the series chopper
Source: created by the authors

2.4 EN55022 Standards

EN 55022 Class A standard for industrial cases gives definite limits for the Quasi-Peak (QP) and Average (AV) detection modes. The thresholds are shown in Figure 7 and are also explained in Table 2. This study, by giving priority only to Class A, guarantees that the EMI profile of the series chopper will be evaluated in the industrial power systems context, where emission limits are higher than those applying to residential or domestic areas.

It specifies conducted disturbance limits within the radio frequency range of 150 kHz to 30 MHz, the limits are expressed on a logarithmic scale in decibels microvolts (dBµV), [14].

The conducted disturbance limits established by EN55022 class A are illustrated in Figure 7.

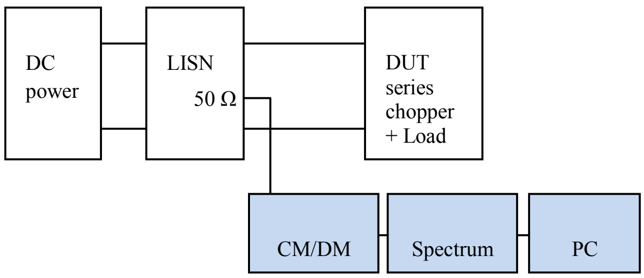

Fig. 7: EN55022 class A, conducted emission
Source: [13], [18]

Table 2 summarizes the conducted EMI limits for each frequency range as specified by the EN55022 standard Class A [24].

Table 2. EN55022 standard limits values

	EN55022 Class A CONDUCTED EMI LIMIT	
Frequency range (MHz)	Quasi-Peak	Average
0.15 to 0.50	80	66
0.5 to 10	73	60
5 to 30	73	60

Source: [13]

2.5 Analytical modeling of EMI sources

2.5.1 Differential Mode (DM) Noise Modeling

The trapezoidal pulse train is the standard switching noise source. Although the physical switching waveforms generally present loss and gain times which are not equal (tr and tf), we still consider setting tr = tf for the sake of getting the analytical solution more easily. This assumption facilitates a strong frequency-domain parameterization that is still valid for EMI prediction since it does not lose the essential notification of the spectral envelope. The DM noise current at the n-th harmonic is mathematically represented in the frequency-domain as follows:

$$I_{DM}(n) = 2Id\left|\frac{\sin(n\pi d)}{n\pi d}\right|\left|\frac{\sin(n\pi t_r / T)}{n\pi t_r / T}\right|$$

Where:

- d is the duty cycle (ton / T).
- T is the inverter switching period.
- I is the peak current amplitude.
- tr is the rise time.
- n is the harmonic order.

2.5.2 Common Mode (CM) Noise Modeling

The CM noise source is modeled in the same way as with an ideal trapezoidal pulse train. Assuming that the rise and fall times are equal (tr=tf), the frequency-domain model of the CM voltage source at the n-th harmonic is given by:

$$V_{CM}(n) = 2V_{dc}\frac{\tau}{T}\left|\frac{\sin(n\pi\tau / T)}{n\pi\tau / T}\right|\left|\frac{\sin(n\pi t_r / T)}{n\pi t_r / T}\right|$$

In this expression:

- Vdc represents the DC bus voltage.
- τ is the off-time of the switch.
- d is the duty cycle of the bottom device.
- n is the harmonic order

3 Results and Discussions

3.1 Measurement of Chopper Disturbances Conducted in CM and DM

The magnetic disturbances produced by the series chopper were analyzed through experiments in both common-mode (CM) and differential-mode (DM) propagation paths, with the EN55022-compliant measurement bench described in Section 2 being used. The purpose of this analysis is to recognize the prevailing disturbance mechanism and to provide a physical explanation for the recorded noise. In order to separate CM and DM components, the voltages measured at the LISN terminals were decomposed based on the classical EMC theory:

$$V_{DM} = \frac{V_L - V_N}{2}, \qquad V_{CM} = \frac{V_L + V_N}{2}$$

where V_L and V_N represent the voltages on the line and neutral conductors measured to ground. The distinction is critical because common-mode or CM disturbances are mostly linked to unwanted capacitive coupling into the ground while differential-mode or DM disturbances result from the current ripple that is circulating through the power loop. The time-domain and frequency-domain representations of CM and DM noise currents as experimentally measured are illustrated in Figure 8 and Figure 9. The difference between the two modes of propagation is clearly noticeable. Even during the entire range of frequency from 150 kHz to 30 MHz, the DM disturbance's magnitude was much greater than that of CM component. The difference in the two types of disturbances can be attributed to the physical layout of the series chopper. The high current transients with their fast rising and falling edges or di/dt associated with the switch-over mainly excite the loop comprised of the MOSFET, diode, and load.

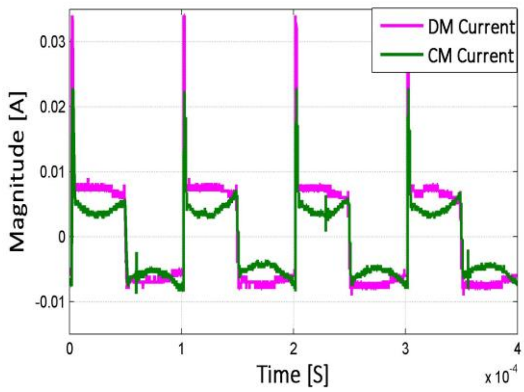

Fig. 8: Measured CM and DM Currents
Source: created by the authors

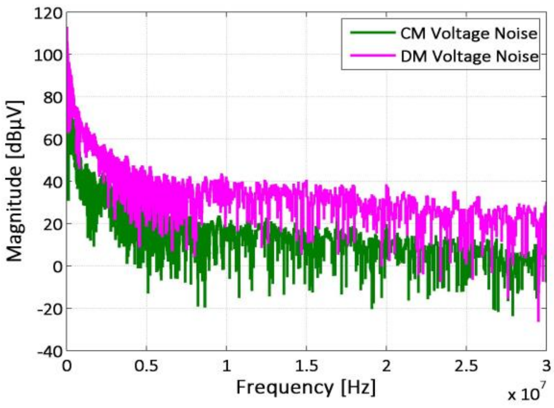

Fig. 9: Measured Spectra of CM and DM Noises
Source: created by the authors

3.2 Effect of Duty Cycle on Chopper EMC Performance

In static converters, EMI is primarily induced by the rapid switching transitions of power transistors. While the switching process is governed by a well-defined duty cycle to ensure proper converter operation, the influence of this parameter on EMC performance is often overlooked. This section specifically addresses that aspect.

The impact of duty cycle variation on DM and CM disturbances was investigated by measuring their amplitudes at both a high duty cycle and a significantly lower one. The CM noise spectrum presented in Figure 10 illustrates the influence of the duty cycle on the CM noise level generated by the chopper.

Experimental results reveal that the CM noise level produced by the chopper at $\alpha = 15\%$ is slightly higher than that obtained at $\alpha = 85\%$. This suggests that lower duty cycles may lead to marginally greater CM emissions, potentially due to differences in switching edge characteristics and spectral distribution of the generated noise.

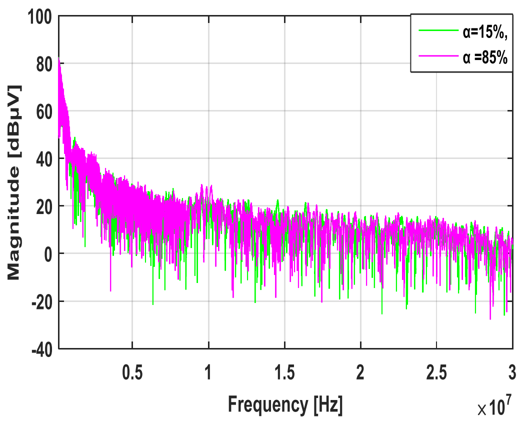

Fig. 10: CM current specter with α=15%, α =85%
Source: created by the authors.

The spectra of noise in differential-mode (DM) depicted in Figure 11 reveals an obvious relationship between the duty cycle of the series chopper and the conducted EMI. From 150 kHz to 30 MHz frequency range, the DM noise level at a low duty cycle (α = 15%) is more than at a high duty cycle (α = 85%) and this is attributed to the increase in current ripple and di/dt at lower duty cycles. The 25–30 MHz band is where this effect is most noticeable as the FET (Fast semiconductor switch) operates with its currents switching very fast, and the loop inductance (which is a power loop parasitic inductance) couples with the current transitions in such a way that they get amplified to high-frequency emissions. For example, at 27 MHz, the measured DM emission is around 30 dBμV at α = 15% while it is approximately 20 dBμV at α = 85%. The data obtained imply that the reduction in duty cycle admits the differential-mode noise to be more intensified, especially in the case of high frequencies that are passed through by the strong excitation of parasitic elements in the power loop.

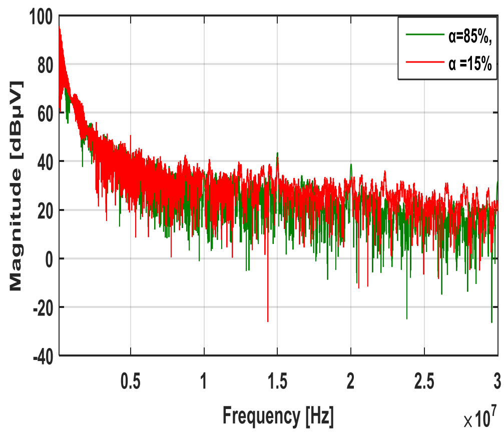

Fig. 11: DM Noise Spectrum Compared with EN55022 Class A Limit
Source: created by the authors.

3.3 Influence of MOSFET Characteristics on Chopper Conducted Disturbances

After examining the influence of propagation mode and duty cycle on the conducted disturbances generated by the chopper, the analysis now focuses on the role of the MOSFET characteristics. The MOSFET is one of the most commonly employed switching devices in static converters, and its electrical and switching properties can significantly affect EMI performance.

To assess this influence, conducted disturbance measurements were performed on the series chopper using two MOSFET models with different characteristics. Table 3 summarizes the key parameters of the IRF840 and IRF540N devices, with particular emphasis on those relevant to EMC considerations.

Table 3. EMC parameters of IRF840 and IRF540N

Parameters	IRF840	IRF540N
Rise time (t_r)	23 ns	40 ns
Fall time (t_f)	36 ns	35 ns
Total gate charge (G_g)	63 nC	71 nC
Max Drain-Source Voltage (Vds)	500V	100V
On-State Resistance R_DS(on)	0.85 Ω	0.044 Ω

Source: [38], [56]

Figure 12 and Figure 13 present a comparison of the CM and DM noise spectra produced by the chopper when using the MOSFETs IRF840 and IRF540N, respectively. The results show that the CM conducted disturbances are very similar for both MOSFETs. In contrast, for DM, the converter equipped with the IRF840 generates significantly higher noise levels than the one using the IRF540N. The distinct EMC characteristics of the different devices shown in Table 3 can explain this difference in EMC behavior. In this case, the main factors are the switching speed and the voltage slew rate. The IRF840 has a faster rise time of 23 ns and thus a higher voltage switching rate of approximately $\frac{dv}{dt} \approx \frac{\Delta V}{t_r}$

The increase in voltage rate goes hand in hand with the increase in currents caused by the movement of charges through the parasitic capacitances of the switching node to ground. The relationship is described by: $i_{CM} = C_p . \frac{dv}{dt}$ where C_P is the parasitic capacitance. The currents of these displacements pass through the LISN and become a part of the measured conducted EMI, especially at high frequencies. Also, quicker voltage transitions are responsible for wider spectral content. In the case of the trapezoidal switching waveform, the high-frequency harmonic noise grows as the rise time decreases, thus the higher noise levels with the IRF840 is a result of the trap. Besides, the gate charge of IRF840 has been a critical factor for it to get the voltage faster, which has been one of the main reasons for the current effect to get more pronounced. On the other hand, the IRF540N, which has a longer rise time and higher gate charge, exhibits less high-frequency spectral content compared to the other device under the same conditions and thus produces lower total conducted EMI.

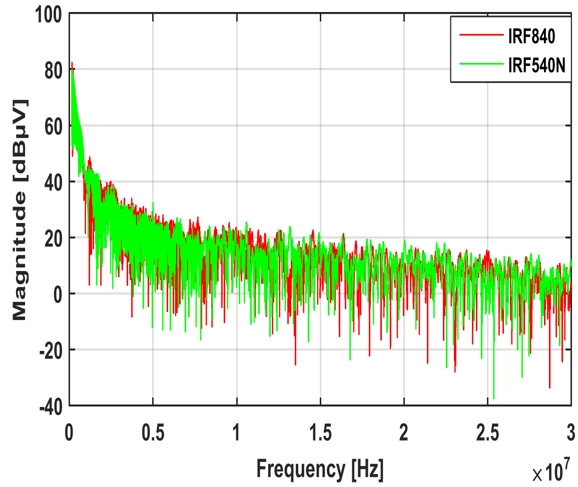

Fig. 12: Measured CM Spectra of IRF840 and IRF540N

Source: created by the authors

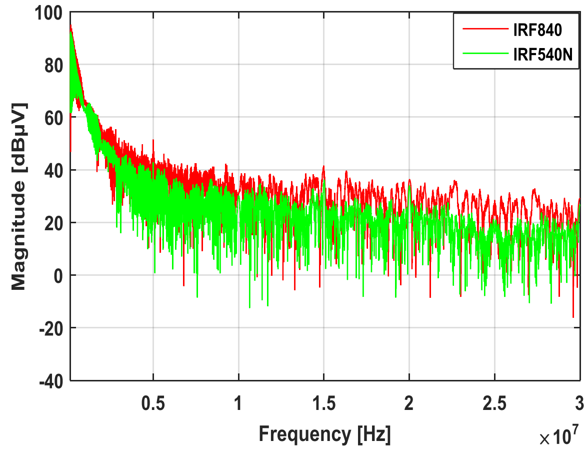

Fig. 13: Measured DM Spectra of IRF840 and IRF540N

Source: created by the authors

3.4 EMC Compliance of the Chopper with Standard EN550022

In modern practice, the design of any electrical machine, device, or component must comply with relevant standardization processes before it can be commercialized.

Figure 14 presents the measured CM noise spectrum of the chopper, compared against the conducted emission limits defined by the EN55022 standard. The results show that the disturbance curve remains consistently below the prescribed limit across the entire analyzed frequency range. This indicates that the converter fully satisfies the EN55022 Class A requirements for conducted emissions.

Consequently, no risk of non-conformity is observed within the evaluated frequency band for CM noise.

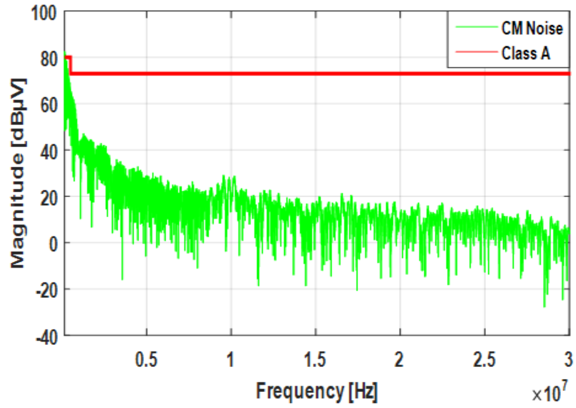

Fig. 14: CM Noise Spectrum Compared with EN55022 Class A Limit
Source: created by the authors

In the differential mode (DM) noise spectrum of the chopper circuit, the Figure 15 shows the data obtained by the measurement compared with the conducted emission limits set by the EN55022 Class A standard. It can be seen from the results of the experiment that the noise levels are not allowed to go beyond the limits at the lower end of the frequency range and the fundamental switching frequency (approximately 150 kHz) of the trapezoidal current source described in section 3.1 is the major contributor of noise at this point. The noise levels drop off and are in line with the standard through the mid-to-high frequency range. The infringement at 150 kHz indicates that although the current design has suppressed high-frequency parasitic ringing effectively, the low-frequency noise—determined by peak current (I) and duty cycle(d)still needs reduction.

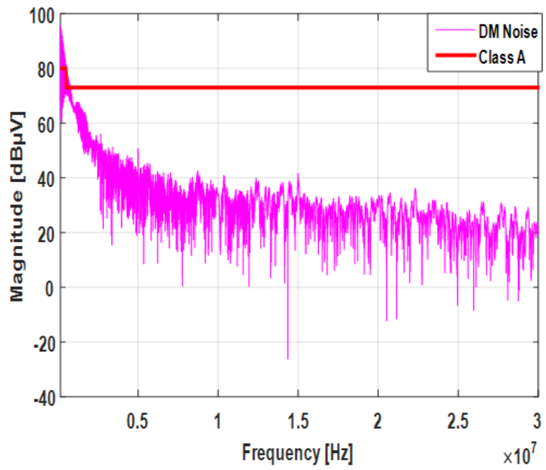

Fig. 15: DM Noise Spectrum Compared with EN55022 Class A Limit
Source: created by the authors

4 Conclusion

The study presented in this paper shows that static converters are a major path for conducted disturbances. The design of this type of converter must therefore take EMC constraints into account, especially for the differential mode, where the conducted disturbances generated by the series chopper are much greater than those of the common mode, and may even exceed the limit authorized by standard EN55022. The EMC analysis must enable the parameterization and dimensioning of several elements such as the duty cycle, the correct choice of transistor and its control parameters. Solutions such as the integration of EMC filters can also be envisaged to remedy these EMC problems.

In short, careful design is needed to ensure electromagnetic compatibility for the chopper in particular and for any static converter, and thus reduce electromagnetic interference.

Acknowledgement:
This work was supported by APELEC Laboratory, Djillali LIABES University, Sidi Bel Abbes, Algeria.

Declaration of Generative AI and AI-assisted Technologies in the Writing Process

During the preparation of this work the author(s) used Quillbot in order to improve the readability and language of the manuscript. After using this tool, the author(s) reviewed and edited the content as needed and take(s) full responsibility for the content of the publication.

References:

[1] Sid Ahmed El Mehdi Ardjoun, Amro Nour, Ibrahim Mahariq. Experimental investigation of conducted electromagnetic interference differential-mode performance in various split-phase induction motors designs, *Results in Engineering*, 17, pp.103–117, (2025). doi: 10.1016/j.rineng.2025.103963.

[2] Yacine Hakmi. Frequency experimental identification approach for single-phase induction motor common-mode parameters. *Electrical Engineering & Electromechanics Journal*, 4, pp.3–7, (2024).

[3] L. Mohamed. Electromagnetic conducted interactions in the inverter-cable-motor system: differential mode, *International Journal of Advanced Natural Sciences and*

Engineering Researches, 43(3), pp.1–10, (2025).

[4] Juntao Yao; Shuo Wang; Zheng Luo. Near Field Coupling's Impact on Radiated EMI and Mitigation Techniques for Power Converters in Automotive Applications. *IEEE Energy Conversion Congress and Exposition (ECCE)* (2020). https://doi.org/10.1109/ECCE44975.2020.9236287.

[5] Benazza Baghdadi, Belhenini Soufyane. Buck Converter Common-Mode Emission with the Frequency Approach. *International Journal of Electronics and Electrical Engineering Systems*, 3(1), pp.24–28, (2020).

[6] Mohamed Miloudi, Houcine Miloudi, Sid Ahmed El Mehdi Ardjoun, IM Elzein, Mohamed Metwally Mahmoud, Wulfran Fendzi Mbasso, Hany S Hussein, Ahmed M Ewais. Comprehensive experimental performance investigation of conducted electromagnetic interference in split-phase induction motors: Common-mode. Journal of Low Frequency Noise, Vibration and Active Control, pp.1-19, (2026). https://doi.org/10.1177/14613484251411703.

[7] Ghalem S., B Abdelber. Prediction of Conducted Disturbances Generated by a DC/DC Converter. *The Eurasia Proceedings of Science Technology Engineering and Mathematics*, 26, pp.507-518, (2023). https://doi.org/10.55549/epstem.1411082.

[8] M. Brahami. Analysis of hybrid photovoltaic system performance, *Advances in Green Energies and Materials Technology*, pp.1–7, (2021).

[9] M. A. Salhi and A. N. Al–Omari. Experimental characterization of the high–frequency isolating power transformer, *Journal of Electrical Engineering and Computer Science*, 86, pp.211–218, (2019).

[10] A. Gourbi. An investigation and analysis of a hybrid photovoltaic system for power supply, Ingeniería Energética Journal, 43(3), pp.1–11, (2022).

[11] Middelstaedt L., Wang J., Stark B. H., & LindemannA. Direct Approach of Simultaneously Eliminating EMI-Critical Oscillations and Decreasing Switching Losses for Wide Bandgap Power Semiconductors, in IEEE Transactions on Power Electronics, vol. 34, no. 11, pp. 10376-10380, Nov. (2019), https://doi.org/10.1109/TPEL.2019.2913223.

[12] Naima M. Characterizing Radiated Electromagnetic Interference from a Power Converter for Improved Electromagnetic Compatibility. *WSEAS Transactions on Circuits and Systems*, 24, pp.135-148, (2025). doi: 10.37394/23201.2025.24.16.

[13] M. El Amine Lahlaci. Analysis of electromagnetic disturbance sources in IGBT and MOSFET circuits in common and differential modes, *International Journal of Advanced Natural Sciences and Engineering Researches*, 4(1), pp.1–10, (2025).

[14] S. Nemmich, M. Oukli, Characterization of conducted electromagnetic interference (EMI) generated by switch mode power supply (SMPS), *Proceedings of ICEE, Batna*, pp.1–5, (2012).

[15] N. Chikhi, Experimental measurement of common and differential modes for variable speed drive DC motor, *Proceedings of IEEE SSD*, pp.1–6, (2022).

[16] Abdelkader Gourbi. Comparative analysis of differential-mode impedance in single-phase induction motors, *WSEAS Transactions on Circuits and Systems,* 23, pp.261–273, (2024). doi: 10.37394/23201.2024.23.26.

[17] Y. Hakmi, Examination of differential-mode characteristics in single-phase induction motors, *International Journal of Advanced Natural Sciences and Engineering Researches,* 4(1), pp.1–10, (2025).

[18] Kharanaq, F.A., Emadi, A., & Bilgin, B. Modeling of Conducted Emissions for EMI Analysis of Power Converters: State-of-the-Art Review, *IEEE Access*, vol. 8, pp.189313-189325, (2020). https://doi.org/10.1109/ACCESS.2020.3031693.

[19] H. Yassine, K. Mendaz, A novel experimental approach for predictive high-frequency modeling of differential-mode impedance in three-phase induction motors, *Proceedings of IEEE ICAEE, SBA*, pp.1–6, (2024).

[20] M. H. Bermaki, H., Transfer function method for EMC high-frequency modeling of electrical machines, *The Eurasia Proceedings of Science, Technology, Engineering and Mathematics, Antalya*, pp.1–8, (2024).

[21] A. Zeghoudi, Experimental measurements of near magnetic field by different probe for AC/DC LED driver, *Proceedings of IEEE EEEIC*, pp.1–5, (2022).

[22] S. Dickmann and S. Schenke, A novel method of transfer–function identification for modeling DM impedance of AC motor, *Proceedings of EMC EUROPE, Angers*, pp.1–5, (2017).

[23] Houcine Miloudi, Mohamed Miloudi. A method for modeling a common-mode impedance for the AC motor, *Elektrotehniski Vestnik*, 84, pp. 241-246, (2017).

[24] Wu S., Ran Z., Tong Z., Liu T., and Lu Y. A Monolithic Integrated E-Mode GaN 48V-to-1V DC-DC Buck Converter with PWM Control, *IEEE International Conference on Integrated Circuits, Technologies and Applications (ICTA)*, Hefei, China, pp.130-131, (2023). https://doi.org/10.1109/ICTA60488.2023.10364290.

[25] Houcine Miloudi, Mohamed Miloudi, Abdelkader Gourbi, Mohamed Hamza Bermaki, Abdelber Bendaoud, Abdelhakim Zeghoudi, A high-frequency modeling of AC motor in a frequency range from 40 Hz to 110 MHz, *Electrical Engineering & Electromechanics Journal*, Vol.6, pp.3–7, (2022).

[26] Carobbi, C.F., & Izzo, D. Evaluation and Improvement of the Reproducibility of CISPR 25 ALSE Test Method, *IEEE Transactions on Electromagnetic Compatibility*, vol. 60, no. 4, pp.1069-1077, (2018). https://doi.org/10.1109/TEMC.2017.2780220.

[27] M. E. Lahlaci, Analysis of Common-Mode and Differential-Mode Noise in DC Motors with Variable Speed Drives, *International Journal of Advanced Natural Sciences and Engineering Researches*, 43, 45–53, (2025).

[28] Li Y., Zhang H., Wang S., Sheng H., Chng C.P., & Lakshmikanthan S. Investigating Switching Transformers for Common Mode EMI Reduction to Remove Common Mode EMI Filters and Y-Capacitors in Flyback Converters, *IEEE Journal of Emerging and Selected Topics in Power Electronics*, vol. 6, no.4, pp.2287-2301, (2018). https://doi.org/10.1109/JESTPE.2018.2827041.

[29] Chuang Bi; Liang Zhao; Rong Hu; Qiang Li; Lin Cheng. Modeling and Prediction of Radiated Electromagnetic Interference for DC-DC Power Converter. *4th International Conference on Energy, Electrical and Power Engineering (CEEPE)* (2021). https://colab.ws/articles/10.1109%2Fceepe51765.2021.9475657.

[30] A. Bendaoud. Réduction des perturbations électromagnétiques conduites dans la machine asynchrone, *Mediterranean Journal of Modeling and Simulation*, 2(1), pp.8–15, (2014).

[31] B. Nassireddine, B. Baghdadi. Conducted differential-mode emission from buck converter, *International Journal of Electronics and Electrical Engineering Systems*, 4(1), pp.24–28, (2021).

[32] Zhang Z., Hu Y., Chen X. et al. A Review on Conductive Common-Mode EMI Suppression Methods in Inverter Fed Motor Drives, *IEEE Access*, vol. 9, pp. 18345-18360, (2021). https://doi.org/10.1109/ACCESS.2021.3054514.

[33] Zhang, B., & Wang S. A Survey of EMI Research in Power Electronics Systems With Wide-Bandgap Semiconductor Devices, *IEEE Journal of Emerging and Selected Topics in Power Electronics*, vol. 8, no. 1, pp.626-643, (2020). https://doi.org/10.1109/JESTPE.2019.2953730

[34] H. Slimani. Common mode conducted electromagnetic interference in inverter-fed-AC-motor, *Electrical and Electronics Engineers Review (EEER)*, pp.271–275, (2010).

[35] Lee Y., Kim D., and Kim J. A GaN Driver IC With a TDC-Based Dead-Time Controller For GaN DC-DC Buck Converters, 20th *International SoC Design Conference (ISOCC)*, Jeju, Korea, Republic of, pp.33-34, (2023). https://doi.org/10.1109/ISOCC59558.2023.10396085.

[36] Abdelber B. Conducted emissions generated by a variable speed drive system, *International Journal of Electronics and Electrical Engineering Systems*, 3(1), pp.24–28, (2020).

[37] Nguyen V.H., Huynh H.A., Kim S., Song H. Active EMI Reduction Using Chaotic Modulation in a Buck Converter with Relaxed Output LC Filter" *Electronics*, 2018, 7, no. 10: 254. https://doi.org/10.3390/electronics710025.

[38] Miloudi M., & Miloudi H. Experimental electromagnetic compatibility of conducted electromagnetic interferences from an IGBT and a MOSFET in the power supply. *Electrical Engineering & Electromechanics*, 3, pp.38–43, (2024). https://doi.org/10.20998/2074-272X.2024.3.05.

[39] Zhang J., Wu C., & Zeng Y. A 11 mV-Undershoot PT Controlled Buck Converter with Adaptive Pulse Train Generator, *IEEE International Conference on Integrated*

Circuits, Technologies and Applications (ICTA), Hefei, China, pp.45-46, (2023). https://doi.org/10.1109/ICTA60488.2023.10364261.

[40] S. Bechkir, S. Hallima, Effectiveness of shielding on the magnetic emissions emitted by a toroidal inductor, in: *Proc. 2nd Int. Conf. on Advanced Electrical Engineering (ICAEE)*, Constantine, Algeria, (2022).

[41] Mohammed Hamza Bermaki, Houcine Miloudi, Mohamed Miloudi, Abdelkader Gourbi, Abdelber Bendaoud, High-frequency Differential Mode Modeling of Universal Motor's Windings. International Journal of Electrical and Electronics Research, Vol. 11, no. 4, pp. 1057-1064, (2023). https://doi.org/10.37391/ijeer.110425.

[42] M.E. Lahlaci, Med miloudi, H. miloudi, Aek Gourbi, M.H. bermaki. Comparative research in common and differential modes of EMI propensity in series and parallel chopper drives for DC motors. Przegląd Elektrotechniczny (7),pp. 151-157, (2025). doi: 10.15199/48.2025.07.24.

[43] A. Tilmatine, L. Canale, Experimental measurement of harmonic distortion and electromagnetic interferences for LED lamps, in: *Proc. IEEE Industry Applications Society Annual Meeting (IAS)*, Detroit, MI, USA, (2022). https://doi.org/10.1109/IAS54023.2022.9940136.

[44] Houcine M. Optimization of EMC Filter for a Variable Speed Drive System in Electric Aircraft. *The Eurasia Proceedings of Science Technology Engineering and Mathematics.* (2023).

[45] H. Slimani, D. Abdelkader, Perturbations en basse fréquence dans les réseaux électriques de distribution, *Proc. 8th Int. Conf. on Electrical Engineering (CEE'2014)*, (2014).

[46] Y. Bellenba. Caractérisation Electromagnétique du Blindage en Champ Proche et Lointain, *Conférence Nationale sur la comptabilité électromagnétique*, pp. 12-20, (2009).

[47] Hamdi R., Hadri Hamida A., Bennis O., On modeling and real-time simulation of a robust adaptive controller applied to a multicellular power converter. *Electrical Engineering & Electromechanics*, 6, pp.48–52, (2022). https://doi.org/10.20998/2074-272X.2022.6.08.

[48] Yadav J.G., Yadav Y. K., and Kumar N. Mathematical Modelling & Simulation of Synchronous Buck Converter and Analysis of Its Simulation Results, *International Conference on IoT, Communication and Automation Technology (ICICAT)*, Gorakhpur, India, pp.1-6, (2023). https://doi.org/10.1109/ICICAT57735.2023.10263672.

[49] S Dickmann, S Schenke, Common mode and differential mode characteristics of AC motor for EMC analysis, International Symposium on Electromagnetic Compatibility-EMC EUROPE, pp. 765-769, (2016). doi: 10.1109/EMCEurope.2016.7739260.

[50] Mohamed Miloudi, Houcine Miloudi, Common and differential modes of conducted electromagnetic interference in switching power converters, *Rev. Roum. Sci. Techn.– Électrotechn. Et Énerg*, Vol. 63(3), pp. 246-251, (2017).

[51] N. Said. Etude et Réduction des Emissions Conduites Générées par l'Alimentation à Découpage (SMPS), *Conférence national sur l'inductique. CI'03*, pp.13-20, (2013).

[52] Muller D., Schweitzer D.N., Beltle M., Tenbohlen S. An Active Common Mode EMI Filter Approach introducing Predictive Pulsed Compensation, *International Symposium on Electromagnetic Compatibility - EMC EUROPE*, Barcelona, Spain, pp.1003-1008, (2019). https://doi.org/10.1109/EMCEurope.2019.8872104.

[53] Zhang J., Lu T., Zhang W., Bian X., & Cui X. Characteristics and Influence Factors of Radiated Disturbance Induced by IGBT Switching, *IEEE Transactions on Power Electronics*, vol. 34, no. 12, pp.11833-11842, (2019). https://doi.org/10.1109/TPEL.2019.2913463.

[54] Juntao Y., Shuo W., and Zheng L., Modeling, Analysis, and Reduction of Radiated EMI Due to the Voltage Across Input and Output Cables in an Automotive Non-Isolated Power Converter, in IEEE Transactions on Power Electronics, vol. 37, no. 5, pp. 5455-5465, May 2022. https://doi.org/10.1109/TPEL.2021.3128628.

[55] Houcine Miloudi, Mohamed Miloudi, Sid Ahmed El Mehdi Ardjoun, Mohamed Metwally Mahmoud, Ahmad A. Telba, Mouloud Denaï, Usama Khaled, and Ahmed M. Ewias, Electromagnetic Compatibility Characterization of Start-Capacitor Single-Phase Induction Motor, *IEEE access*, vol. 12,

pp. 2313-2326, (2024). doi: 10.1109/ACCESS.2023.3349018.

[56] S Nemmich, H Slimani. Analysis and reduction of common-mode and differential-mode EMI noise in a Flyback switch-mode power supply (SMPS), *Telecommunications Forum (TELFOR)*, 1080-1083, (2012). doi: 10.1109/TELFOR.2012.6419398.

[57] Bouaziz Laila, Dhaoui Mehdi, Ben Hamed Mouna, Optimal Energy Management and Control of a Hybrid PV/Wind System with Storage Integration, *WSEAS Transactions on Circuits and Systems,* vol. 24, pp. 112-119, (2025). doi: 10.37394/23201.2025.24.13.

[58] Khoukha Bouguerra, Samia Latreche, Mabrouk Khemliche, Hamza Khemliche, Fuzzy Sliding Mode Control of the Photovoltaic System Connected to the Network, *WSEAS Transactions on Circuits and Systems*, vol. 24, pp. 41-50, (2025). doi: 10.37394/23201.2025.24.5.

[59] Lahmani, A., Bennihi, S.M., Bendaoud, A. Experimental Characterization of Conducted EMI in DC/DC Buck Converters: Effects of Duty Cycle and Switching Device, Jordan Journal of Electrical Engineering, 2025, 11(4), pp. 705–719. https://doi.org/10.5455/jjee.204-1757601934.

[60] Mohamed Mankour, Leila Ghomri, M'hamed Sahnoun, "Improvement of AC network performance using shunt and hybrid FACTS devices," Energy Management Systems for Microgrids with Wind Pv and Battery Storage, 2025, pp. 43–66. https://doi.org/10.1049/PBPO270E.

[61] Lahlaci, M.E.-A. Investigation of Conducted Electromagnetic Disturbances in Power Electronics: A Case Study on DC/DC Choppers. *Eurasia Proceedings of Science Technology Engineering and Mathematics,* 2025, 38, pp. 81–89. https://doi.org/10.55549/epstem.1204.

[62] Mohamed Mankour, "Experimentally Validated Modular-Terminal-Behavioural Modelling of Conducted EMI in Full-Bridge Inverters," *Electrotehnică, Electronică, Automatică (EEA),* 2026, vol. 74, no. 2, pp. 64-72. doi: https://doi.org/10.46904/eea.26.74.2.1108008.

[63] Med Hamza B. Expermental Evaluatin of the EMC Behavior of LED Lamps. *IEEE Sustainbale Smart Lighting Word Conference and Expo.* LS25 2025. https://doi.org/10.1109/LS2566125.2025.11467637.

[64] Houcine M., Mendaz, K. Electromagnetic Interference (EMI) in Variable-Speed AC Electric Drives: *Mechanisms and Solutions. Eurasia Proceedings of Science Technology Engineering and Mathematics,* 2025, 38, pp. 12–19. https://doi.org/10.55549/epstem.1197

[65] Zhai L., Zhang T., Cao Y., Yang S., Kavuma S., & Feng H. Conducted EMI Prediction and Mitigation Strategy Based on Transfer Function for a High-Low Voltage DC-DC Converter in Electric Vehicle. *Energies journal*, 11, pp.55-80, (2018). https://doi.org/10.3390/en11051028.

[66] Laour M., Tahmi R., & Vollaire C. Modeling and Analysis of Conducted and Radiated Emissions Due to Common Mode Current of a Buck Converter, *IEEE Transactions on Electromagnetic Compatibility*, vol. 59, no. 4, pp. 1260-1267, (2017). https://doi.org/10.1109/TEMC.2017.2651984.

Contribution of Individual Authors to the Creation of a Scientific Article (Ghostwriting Policy)

The authors equally contributed in the present research, at all stages from the formulation of the problem to the final findings and solution.

Sources of Funding for Research Presented in a Scientific Article or Scientific Article Itself

No funding was received for conducting this study.

Conflict of Interest

The authors have no conflicts of interest to declare.

APPENDIX

Table 1. Literature review for EMI DC-DC converters

Reference	Converter type	Realization of converter	EMI predicted type	Method of prediction	Mitigation method	Parameters investigated
[4]	Chopper serie	✓	Radiated	Direct experimental measurement	Optimizing PCB layout	Switch
[7]	Chopper serie	x	Conducted	Indirect	x	α, tm, *f*, td
[12]	Flyback converter	x	Radiated	Direct experimental measurement	NA	CM choke impedance
[32]	Boost converter	x	Conducted	Experimental measurement	Filter	x
[38]	Chopper serie	x	Conducted	Indirect experimental measurement	x	NA
[50]	rectifier	✓	Conducted	Indirect experimental measurement	HF Filter	NA
[65]	Isolated full bridge	✓	Conducted	Indirect experimental measurement	HF Filter	NA
[66]	Chopper serie	x	Conducted	Indirect experimental measurement	x	MOSFET, IGBT

Source: created by the authors